BVRI photometry of M34

Julia Frothingham, Alyssa Guzman, Molly Loughney, Jingyi Zhang

Abstract

CCD photometry of open cluster M34 was carried out on the Smith College 16-inch telescope with BVRI filters. These data were used to create unique color-magnitude diagrams for several combinations of filters. The age of the cluster was determined through isochrone fitting to the CMDs and compared to previously reported values. The distance of the cluster was determined using the distance modulus equation and isochrone shifting. It was found that M34 is approximately 300 million years old, and 501 parsecs from Earth.

Introduction

A Hertzsprung-Russell (HR) diagram is a plot of stellar luminosity against temperature. The y-axis is the luminosity, measured either in units of power or in relation to a specific star's luminosity, such as the sun. The x-axis is the temperature of the star, inverted such that higher temperatures are in the leftmost part of the HR diagram and lower temperatures are in the rightmost part of the HR diagram. The Hertzsprung-Russell diagram provides important information relating the luminosity of stars, or the rate at which they emit energy, to their temperatures. It is also extremely useful in grouping stars by their stage of life, as stars exhibit different behaviors based on their age.

The most prominent feature of an HR diagram is the main sequence. This is a curve of hydrogen-burning stars with correlated luminosities and temperatures. For stars on the main sequence, high luminosities correspond to high temperatures, and low luminosities correspond to low temperatures. But the HR diagram shows stars in other regions as well. It displays a turn-off point along the main sequence, where formerly hydrogen-burning stars begin burning helium instead. The turn-off point will be in a different place along the main sequence depending on the age of the cluster. Hot, bright stars are larger and burn through hydrogen at a much faster rate than smaller, dimmer, colder stars. These stars evolve off the main sequence quickly after they are formed, so older clusters will show a turn-off point that is dimmer and redder compared to younger clusters. Along the turn-off point and its associated branch, the luminosity of a star increases as the temperature decreases. The branch leads to groups of supergiant and red giant stars with high luminosities and medium to low temperatures, burning elements other than hydrogen and expanding. Once these red giants and supergiants have burned through each element up to iron, they can no longer support themselves with fusion in their core. They become white dwarfs, neutron stars, or black holes depending on their initial masses. HR diagrams can show white dwarfs, stellar cores with low luminosities and high temperatures.

A color-magnitude diagram (CMD) is the precursor to an HR diagram. It is a plot of stellar brightness in magnitudes against color index. In contrast to the HR diagram, the quantities on the CMD axes come almost directly from measured data. The axes of a CMD are determined from CCD (charge-coupled device) images of stars taken in multiple wavelength bands. The y-axis is stellar brightness in a particular wavelength band. The x-axis is the color index. The color index is determined by comparing the strength of the star's emission in two wavelength bands. For CMDs, this is done by finding the difference between CCD counts (proportional to the number of photons received from the star) in each wavelength band. Using a standard star of known magnitude, total CCD counts in a specific wavelength band are transformed into magnitudes. Through aperture photometry, the flux, or energy rate per unit area, is

calculated from the image exposure time and number of counts within a certain area of pixels corresponding to a star. This flux, and the known magnitude of the standard star, can be used to calculate the magnitude of each star in the image in different wavelength bands. The CMD displays the same general trends as an HR diagram, but the plotted quantities cannot be used directly to determine physical properties, though they are useful for qualitative comparisons of the stars in the cluster.

Generating a color-magnitude diagram (CMD) from flux-calibrated photometry tables requires the use of a standard star. The magnitudes listed in the photometry tables are instrumental magnitudes--they are dependent on the specific instrument used as well as observing conditions. In order to be compared to the results of other observations, these magnitudes need to be converted to the standard apparent magnitude system relative to Vega.

The definition of an apparent magnitude is as follows:

$$m = -2.5\log_{10}(F) + c$$

where m is the apparent magnitude of the object relative to Vega;
F is the flux, or energy rate per unit area, received from the object;
c is a "zero-point" quantity to scale the received flux to a standard magnitude scale;

For a CCD, the number of counts received by the detector is proportional to the number of photons received from the target. So the ratio of total counts N to image exposure time t_{exp} should produce the same quantity as flux, and can be used to calculate the magnitude of the target. This quantity is known as the instrumental magnitude m_{inst}.

$$m_{inst} = -2.5\log_{10}(N/t_{exp})$$

However, the instrumental magnitude is not scaled to a standard system. This is where the zero-point is necessary. It is a filter-dependent quantity in magnitude units that describes how much the instrumental magnitude for a target in a given filter needs to be offset in order to match the standard apparent magnitude of a target in that filter. This standard apparent magnitude, or calibrated magnitude m_{cal} is equal to the sum of the instrumental magnitude and the zero-point magnitude m_{zp}.

$$m_{cal} = m_{inst} + m_{zp}$$

The standard star, by definition, has a known apparent magnitude in each filter. So the zero-point magnitude for each filter can be calculated by subtracting the standard star's instrumental magnitude in each filter (calculated from our own measurements in photometry tables) from the standard star's calibrated magnitude in each filter (given in standard star catalogs). The zero-point magnitude for each filter can then be added to the instrumental magnitudes for each star in each filter (calculated from information in photometry tables) to produce a calibrated apparent magnitude for each star in the image in each filter. These apparent magnitudes can then be used to generate y-axis magnitudes and x-axis color indices for CMDs.

To transform the CMD into an HR diagram, the color index along the CMD's x-axis can be related to temperature through the concept of blackbody radiation and the Planck function. A blackbody is an object

that radiates all light that it absorbs. Its spectral radiance can be described by the Planck function, which relates spectral radiance to temperature, wavelength of emitted photons, and various constants. Different temperatures will produce different "peak wavelengths", wavelengths at which emission is strongest. Though stars are not ideal blackbodies, they behave similarly enough that comparing the strength of stellar emission in different wavelength bands to the peak wavelength of Planck function models can provide an estimate for temperature, the x-axis of an HR diagram. A standard star with known luminosity is used to relate magnitudes, from total CCD counts, to luminosity.

Star clusters can yield very informative CMDs and HR diagrams for studying stellar evolution. Star clusters are groups of stars that were formed at the same time from the same material. The stars in a cluster are also all roughly the same distance from Earth. Properties such as brightness can be dependent on multiple factors. Because so many of their properties are the same, it is convenient to compare the stars in a cluster to see how factors other than age, distance, and composition impact stellar brightness, color, and size. Globular clusters are typically much older and contain thousands to millions of stars that remain gravitationally bound in a roughly spherical shape. Open clusters are typically younger and smaller, containing hundreds to thousands of stars. The stars in an open cluster are more loosely gravitationally bound, and so can spread out into unusual shapes. An open cluster, M34, was chosen as our observing target because it is less dense than a globular cluster and therefore it can be easier to resolve and identify individual stars.

An isochrone is a model of color and brightness over the course of stellar evolution that shows how the stars in a cluster will have progressed by a certain age. Stellar evolution is dependent on initial mass. All stars begin on the main sequence, burning hydrogen. Higher mass stars are located on the brighter, bluer portion of the main sequence and burn through their hydrogen at a much greater rate than lower mass stars, so higher mass stars leave the main sequence quickly and begin burning helium and heavier elements sooner than lower mass stars. So an older isochrone would show more stars on the Red Giant Branch, while a younger isochrone would show more stars only on the main sequence. Isochrones are used to estimate the ages of star clusters. Isochrones for different ages are generated programmatically from the approximate initial stellar masses in the cluster, then the isochrones are fitted to an HR diagram or CMD. The diagram should closely match the isochrone corresponding to the age of the plotted cluster.

Procedures

The telescope used for this observation was the 16-inch Meade LX200-ACF telescope with the SBIG STL-6303 CCD camera located at Smith College's Observatory (latitude 42:19:02 N, longitude 72:38:22 W). This camera is used to create high quality images and is more sensitive to light than other digital cameras, which is why it's essential to use this to capture light from faint stars. This camera has UBVRI filters. The telescope is a Schmidt-Cassegrain telescope, which means that the telescope is a combination of one primary concave mirror and a secondary convex mirror. The telescope was on an equatorial mount which is the structure that holds the telescope in place and it's at an angle pointing to Polaris, the north star. The field of view for this telescope is 15' x 24' and our pixel scale is 0.435.

The observation took place on October 28, 2021 from 22:00 to 24:00. No moon during the time of observation. Measuring from the dome, the temperature was 4 degree Celsius (40 degree Fahrenheit), and humidity was 72%. The sky was clear during the first half of the observation, when all the M34 data

frames were taken. Cloud and fog started at around 23:30, the dome was closed and no more data frames were taken. Wind speed near the ground was around 5mph during the time of observation. (Data obtained from https://www.timeanddate.com/weather/@4945819/historic?month=10&year=2021) Strong winds might have been present in the upper atmosphere as the twinkling of stars can be clearly seen by human eyes. During the time of observation, the seeing was around 7-8 pixels, which corresponds to roughly 4 arcseconds. The seeing was estimated from the full width at half maximum (FWHM) of the test image during setup.

After we had performed our observations, we took our raw images and calibrated, aligned and combined them to create reduced images of our objects which we could then analyze to create our CMDs. The first step of this calibration process consists of the reduction of our bias frames. Bias frames are images taken with an exposure time of zero seconds and no light exposure, and they represent the signal from the detector caused by the voltage of the analog to digital converter or random electron movements in the semiconductor structure of the CCD. During our observation night, we took five of these bias frames, which we then later combined into a master bias frame by creating a 3 dimensional array, populating this array with our bias frame data, and taking the median of the new array. We took the median of the frames as it better accounts for outlying data than the mean average as is shown in figure 1.

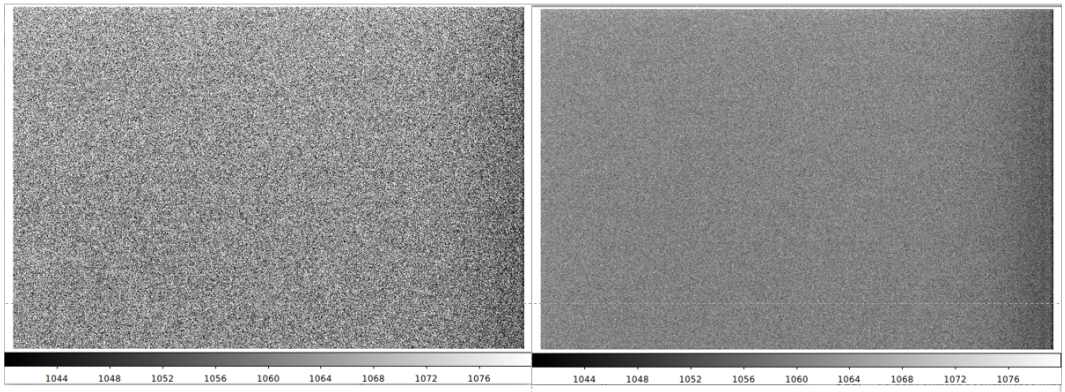

(a) Figure 1 (b)

(a) Raw bias frame. (b) Combined master bias frame. The grey scale of both image is set to between 1040 to 1080. After the median combination, random fluctuation in the image is reduced. The master frame is more uniformed than the raw image.

After we created our master bias frame, we then reduced our dark frames. Dark frames are images taken over a long exposure time with the detector covered so that no light reaches it, and they represent the noise generated by thermal electrons or manufacturing differences, which appear as noise across the whole image, as well as pixel damage and cosmic rays which show up as “hot spots”. Our dark frames were taken over a 60 second exposure, and to reduce them we began by subtracting our master bias frame from each raw dark frame in order to remove the effects from the noise already accounted for by the bias. We then median combined these bias-subtracted dark frames to create our master dark frame for the same reason detailed earlier. As shown in figure 2, this process changes the average pixel value of the dark frame from an order of 10^3 to an order of 10^1-10^2 and visually removes many obviously noisy pixels.

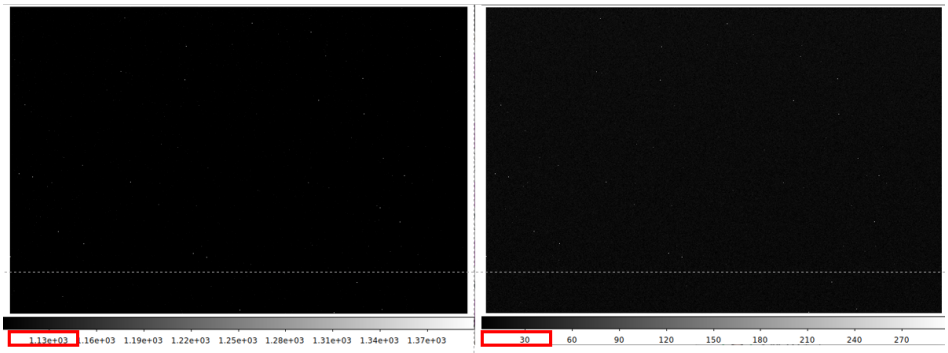

(a) Figure 2 (b)

(a) Raw dark frame, 60 second exposure. (b) Bias subtracted master dark frame, 60 second exposure. Note that the pixel value in the raw image is around 1000, and the pixel value in the master frame is around 100. The smaller number is the thermal noise accumulate

We also divided our master dark frame by its exposure time in order to create a master dark that has an "exposure" of 1 second. This master dark frame can then be multiplied by the exposure time of our other images to scale it appropriately. As dark current accumulates with time, we need to ensure that the exposure times of the dark frame and image we hope to process are the same.

Once we had created our master dark and bias frames, we began reducing our flat field images. Flat fields are a normalized amount of light hitting our detector with various exposure times, depending on the detector and filter. We achieve this normalized amount of light by covering the telescope aperture with a white sheet and shining a light on it, so theoretically the same number of photons should hit each pixel. Flats measure the sensitivity of each pixel and allow us to correct for noise such as imperfections on the telescope lens (dust, scratches, optical imperfections) and the quantum efficiency, or ability to convert photon energy to electron movement, of each pixel. We subtracted the master dark and master bias frames from our raw flat fields for each filter, after scaling the master dark so its exposure matched that of each flat. The reasoning for this step is the same as the reasoning for subtracting the master bias from each dark frame; it ensures the master flat frame represents only noise from the flat exposure.

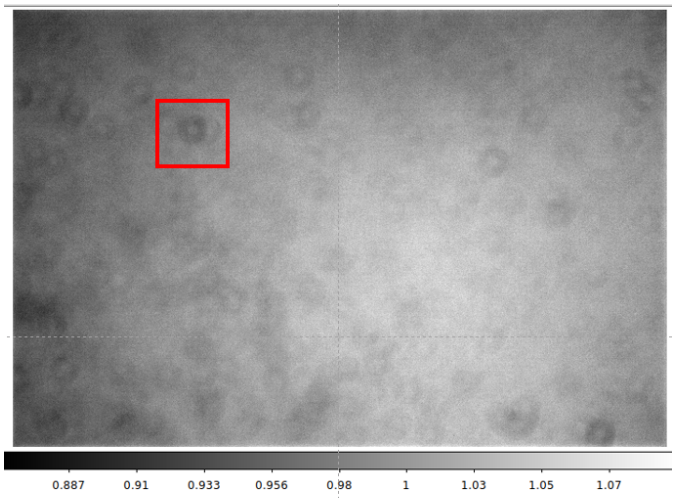

Figure3

Master flat field in B filter. The field has been normalized. The dark donut shape corresponds to the dust on the reflective mirror. The edge of the image is darker than the middle. Dividing the data frames with the normalized flat field remove the gradient and the darkening caused by the dust.

After the flat fields had been bias and dark subtracted, we once again median combined them into a master flat field frame. However, unlike the previous master frames, we normalize the flat field images before combining them and taking the median. As seen in figure 3 this process changes the pixel values of the flat fields from an order of 10^4 to an order of 10^{-1} and makes features such as the donuts created by dust on the telescope lens or the vignetting from the lens shape more obvious.

The final step of our calibration process was applying the master calibration frames to the images of the objects we wanted to analyze. We did this by first subtracting the bias and dark masters from our science images, and then dividing these images by the master flat. We divide by the flat field as its noise represents distortions to the image instead of background noise in the detector, so we cannot just remove the value of those pixels through subtraction. Figure 4 shows a comparison between a raw image of our cluster and the same image once reduced. As you can see, the reduction process changes the average pixel value by about a factor of 10^2 and creates clearer stars in the image. The background noise levels are more standardized, and a gradient that was present in the raw image, likely from the dark frame, is removed.

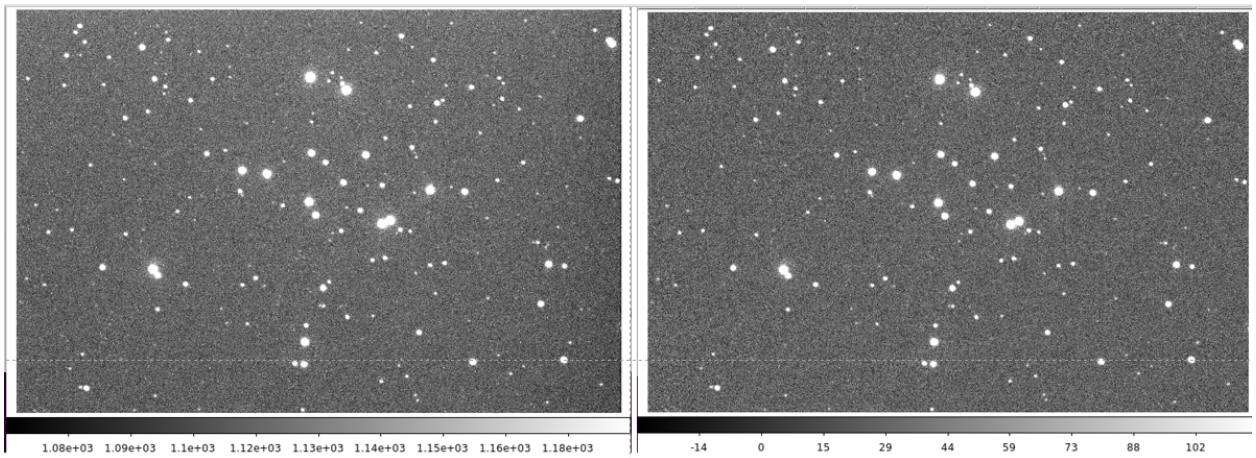

(a) Figure 4 (b)

(a) Raw data frame in B filter. (b) Same data frame, fully reduced. Note that the gradient on the very right of the raw image is removed by diving the flat field.

The next step in our image reduction process was the alignment and combination of our science images to create one image from which we can extract our data to analyze. This combination reduces the signal-to-noise ratio, or SNR, of the final image as well as makes fainter objects easier to see. To do this we first picked several reference stars and located them in each image, then we calculated the centroid of these reference stars. We calculated the centroid by choosing a star and a patch of background and then took an image substamp, or smaller array around each part of the image. We then took the background values and found their mean and standard deviation, and found the value of 3 times the standard deviation to create a background limit. This limit will determine which pixels count as “star” and which pixels count as “background” when we try to calculate the centroid. We then subtracted the background limit from our star array to determine which pixels are the star, and discarded any pixels that had a value of 0 or lower which would indicate that they were part of the background signal. We summed our remaining pixel values together as well as summing the pixel values multiplied by their coordinates, once for x and once for y, and divided the multiplied sum by the total sum to find the x and y coordinates of the centroid of our star. With the centroid of our reference image, we took the centroid of the same star in our other images and subtracted our reference image centroid coordinates from each of the other centroid coordinates to determine the shifts of each image.

Once we had the shifts for each image, we aligned them. We did this by first padding each image and filling the padding region with an arbitrary value to ensure that we did not cut off any desired information when shifting the images. We then shifted the images according to our previously calculated shifts. We shifted the images using the interp.shift function from the scipy.ndimage package for multidimensional image processing. We can then median combine our shifted images to produce our final image, from which we can extract photometry data.

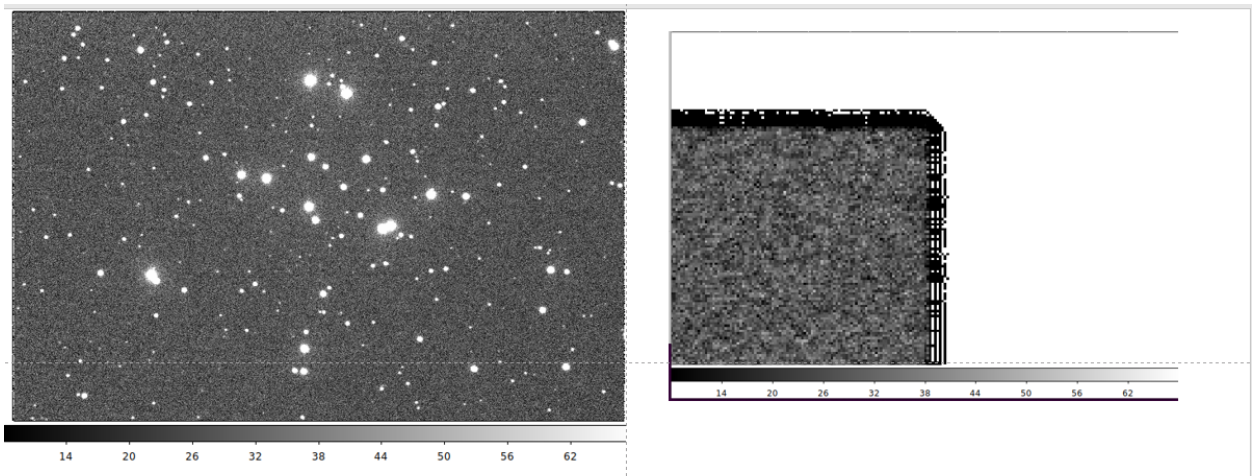

(a) Figure 5 (b)

(a) Combined image in B filter of M34. (b)The edge of the combined image, zoomed in. The dark strip are the padding region that allows the images to shift and combine without losing any data.

In order to find the magnitudes of the stars in our cluster, which will allow us to create our CMD, we need to perform aperture photometry on our images. Aperture photometry allows us to determine how much of our signal is coming from the star and how much is coming from the background by subtracting a near background signal from the star signal, thus theoretically isolating the signal from the flux of our star. Before we could do this, we needed to decide what signals were star signals, and what was background. We did this by choosing a value to multiply the standard deviation of the background values, which provided a background limit. For our cluster images, we experimented with a few different values for the limit below which we would consider the signal part of the background, called nsigma, to try and ensure we were extracting enough stars to build a CMD with a recognizable structure but not accidentally including signal that was not actually a star, which could prevent us from successfully identifying our CMD structure, thus introducing error into our later analysis. We first used an nsigma value of 5, which identified 327 stars in the B filter, 473 in the V and R filters and 396 stars in the I filter. Upon visual inspection, this value seemed to include all visual stars in the image, although it was perhaps over-sensitive as some background areas were included as well. A slightly larger nsigma of 7 identified 254 stars in the B filter, 402 in the V filter, 405 in the R filter and 338 stars in the I filter, and though it still detected a few background areas as stars, particularly on the edges of images, we found it to be acceptably sensitive for our purposes and so we chose to use this value to create our star catalog. For our standard star image, we chose an nsigma value of 15, which identified all visible stars and did not include any false detections. For both our cluster and standard star images we chose to use the catalog generated by the B band images, as these were the smallest catalogs, and so we decided they included the fewest number of false detections. The full width at half maximum value for each image was determined in AstroImageJ (AIJ). Using simbad, we verified the position of our standard star as indicated in figure 6.

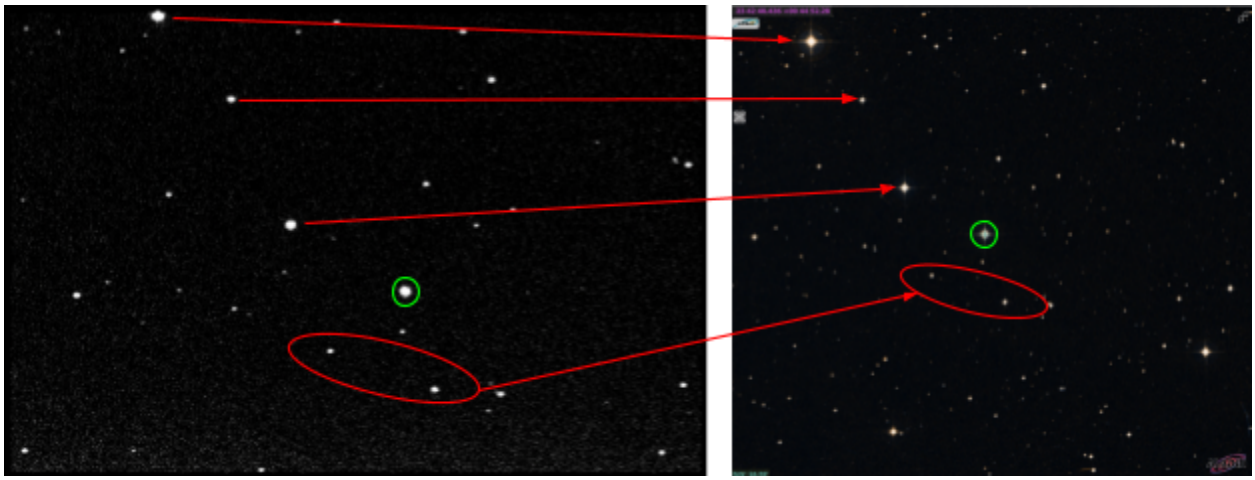

Figure 6

Comparison between our image of SA 115271 taken in the V-band (on the left) with an image of the same star captured from SIMBAD (on the right). Identifying features have been paired across each image, while SA 115271 is circled in green. Note that our image has been inverted in the y direction in order to match the orientation of the SIMBAD image.

Once we believed that we had isolated the signal coming from our stars, we extracted the photometry from the image in order to obtain a value for the flux of each star in our cluster. We did this by using an inner aperture and outer annuli to distinguish between the signal coming from our star and the background signal. The radius of aperture and sky annuli was determined from AstroImageJ. (Table 1, Figure 7) Once we had done this, we obtained the flux for each star in the image by reading the pixel values for each star and dividing these values by the exposure time of the image. We then took the flux values from our standard star and calculated our instrumental magnitudes. The instrumental magnitude represents the magnitude of the star dependent on the instruments that were used and are calculated using the equation

$$m_{inst} = -2.5 log_{10}(F) \text{ where } F = \frac{N}{t_{exp}}$$

We compared the instrumental magnitudes of our standard star to the known magnitude values in each filter, which allowed us to find our instrument's zero point magnitude in each band by subtracting the instrumental magnitudes from the known magnitudes, these results are summarized in table 2. Using these zero points, we calculated the calibrated magnitudes of our cluster data by adding the zero points to the instrumental magnitudes. Since we took the image of our standard star and M34 under similar conditions, we can minimize atmospheric, instrumental or other effects on our magnitudes, and so we can assume the calibrated magnitudes that we calculate are representative of the actual apparent magnitudes of our cluster. Using this data, we then generated our final CMDs.

Name	Filter	FWHM (pixels)	Aperture radius (Pixels)	Sky annuli inner radius (Pixels)	Sky annuli outer radius (Pixels)
SA115271 (Standard Star)	B	18*	10	35	53
SA115271 (Standard Star)	V	9.91	16	28	42

SA115271 (Standard Star)	R	8.01	15	27	41
SA115271 (Standard Star)	I	7.58	14	25	38
M34	B	8.24	14	25	38
M34	V	10.91	15	27	41
M34	R	8.84	14	25	38
M34	I	9.30	14	25	38

Table 1

Full width at half maximum (FWHM) and aperture parameter of the standard star and M34 in four different filters. * Note that the FWHM value of the standard star image in B band is arbitrarily set. The shape of the star in this image is stretched in the x axis, and the normal FWHM value given by AIJ would be too small for the algorithm to recognize the position of the star.

B	V	R	I
10.31 +/- 0.0005	9.695 +/- 0.0005	9.342 +/- 0.0005	8.993 +/- 0.0005

Table 2

Actual apparent magnitude of SA115271 (the standard star.) in each band. The magnitude value is from the Landolt standard star catalog[1], the uncertainty is obtained from SIMBAD.

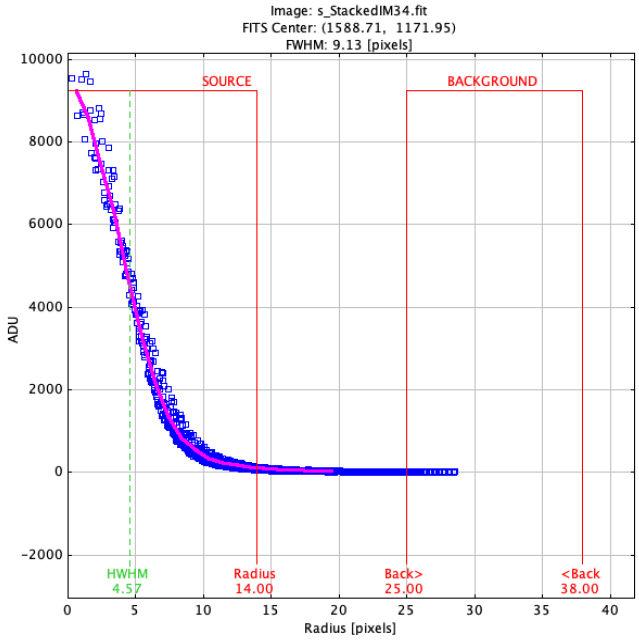

Figure 7

We determined the FWHM and aperture parameter in each image using AIJ. The figure shows the seeing profile of one star in M34 in the I band. We examine multiple stars' FWHM in the same field, and the average is used to search for stars.

[1] Accessed from European Southern Observatory (2010) at https://www.eso.org/sci/observing/tools/standards/Landolt.html. With reference to Landolt (1992).

Results

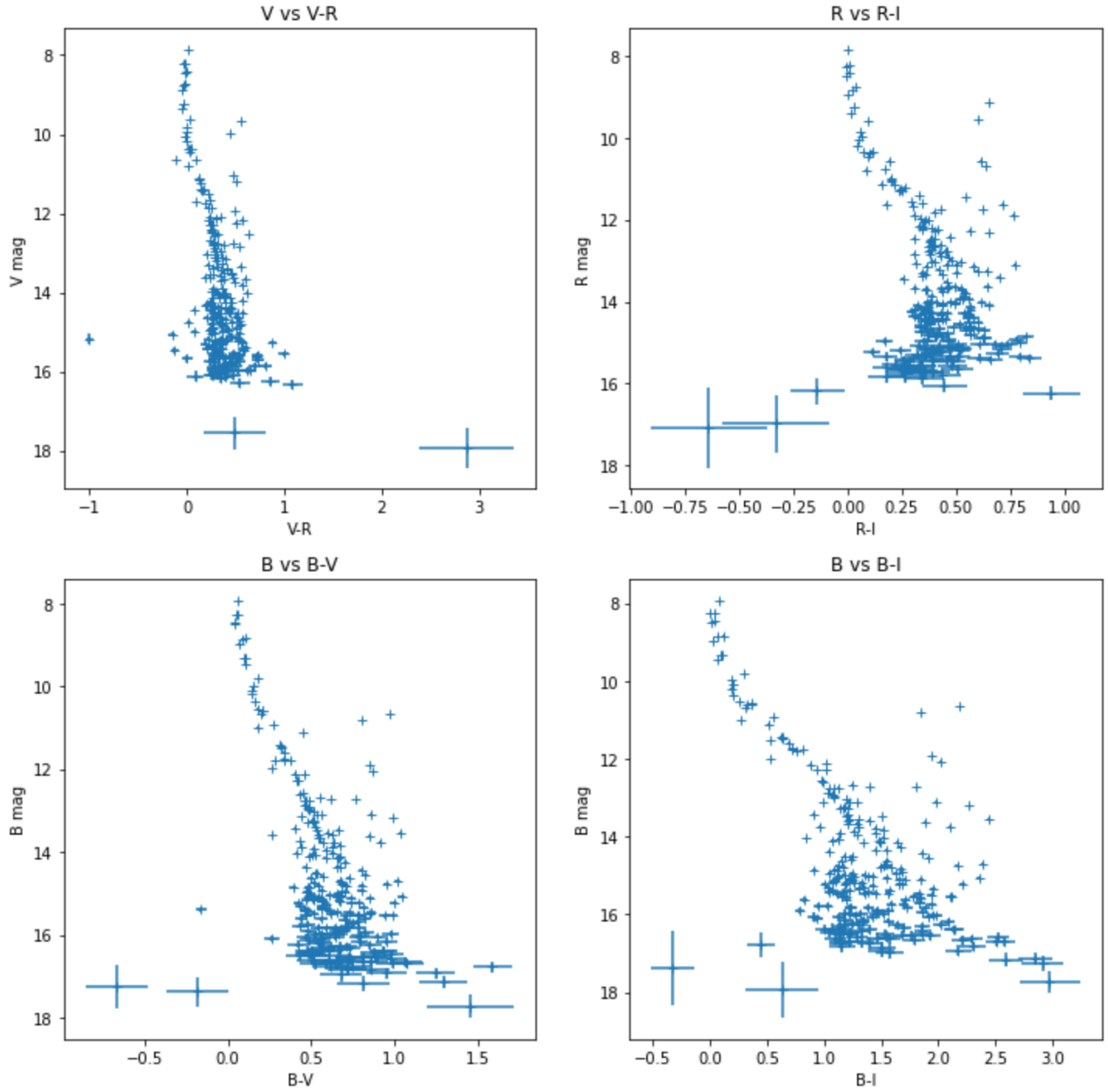

Figure 8

Color-magnitude diagrams (CMDs) generated from reduced, aligned, combined, and magnitude-calibrated data for M34. Each CMD plots a unique combination of color index and apparent magnitude from the filters used. All four CMDs show the same approximate range of magnitudes along the y-axis, with the main sequence ranging from about 8 mag to about 17 mag in the B, V, and R filters. All CMDs show a clear main sequence from top left to lower right.

We obtained the color indices and apparent magnitudes of the 254 star detections in M34. The four color-magnitude diagrams shown in Figure 8 display similar features to one another. They all show a prominent main sequence containing most of the stars in the image.The shape of the CMDs are slightly different, as the color index would be more spread out between filters with larger wavelength difference. All CMDs have a smaller number of stars distinctly to the right of the main sequence, and a few stars in the bottom left corner of the CMD with larger error. It's possible that those stars are white dwarfs, while the stars to the right of the main sequence are red giants. However, the stars to the right of the main

sequence appear to form a distinct branch. It is more likely that these stars are not part of the M34 cluster, but are instead stars from a different cluster, or field stars not part of any single cluster. The dim stars at the bottom left may be false detection generated by the algorithm.

Isochrone fitting

To determine the age of our cluster, we used isochrone fitting. Provided with several isochrones generated by CMD 2.2[2], we first plotted the isochrones over our CMD (Figure 9). We initially chose an isochrone with an age of 300Myr, as from a visual analysis of our CMD we made the assumption it was a younger cluster due to its lack of an obvious late turnoff point. However, there were some data points that were off the main sequence in our CMDs, meaning that some stars could have begun their main sequence turn offs in our cluster.

We loaded in the data for the 3Myr isochrone and calculated its V-R magnitude values in order to plot it against our V vs. V-R magnitude CMD. We chose the V vs V-R data to carry out isochrone fitting because the V and R bands are much less susceptible to extinction effects that could shift the color indices of the CMD to the right. These effects are more prominent in the smaller wavelength of the B band. This initial plot showed that while the shape of the isochrone could be close to our CMD, we would need to shift the position of the isochrone to better assess. The reason for the shifting is due to the fact that the isochrones are plotted using absolute magnitudes, while the CMD is plotted using the apparent magnitude. Using visual inspection as well as trial and error, we determined that we should shift the isochrone by 8.5 magnitudes in the y-axis (Figure 10). This shift aligned our CMD plot with the isochrone plot.

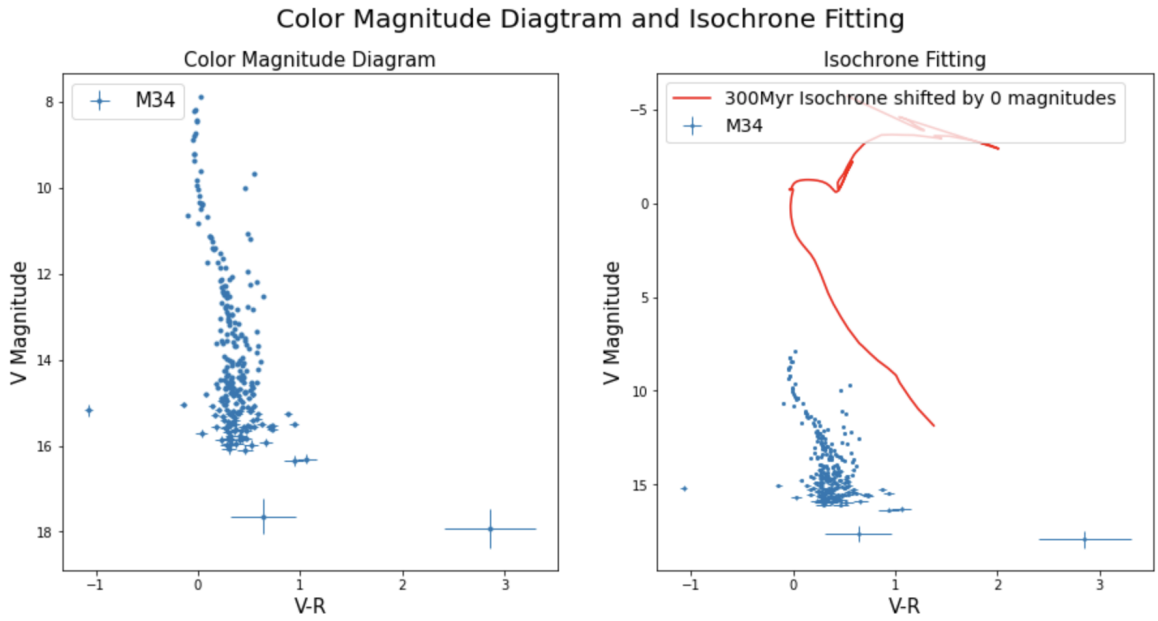

Figure 9

V vs. VR color magnitude diagram for our cluster (left) against the same plot with the 300Myr isochrone plotted over it (right). Note that the isochrone is significantly "brighter" than the CMD. This is because the isochrone shows the absolute magnitude of the stars (the apparent magnitude of stars if they were 10pc away), while the CMD displays the apparent magnitude we measured.

[2] CMD 2.2 (http://stev.oapd.inaf.it/cmd). With reference to Marigo et al. (2008, A&A 482, 883), + Bertelli et al. (1994, A&AS, 106, 275), cf. Maiz-Apellaniz 2006 + Bessell 1990, and Loidl et al. (2001).

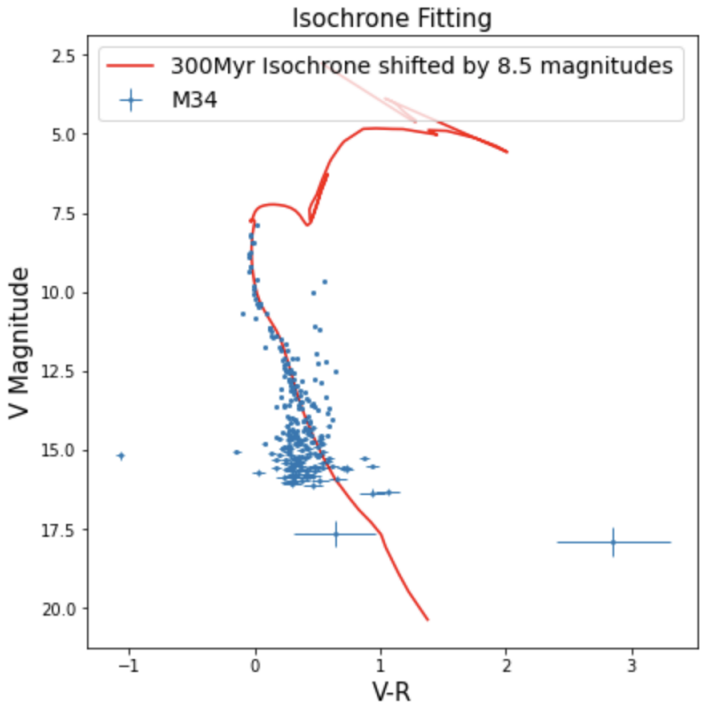

Figure 10.
The 300Myr isochrone aligned with our V vs. V-R CMD by shifting the isochrone V magnitude values down by 8.5.

We also tested other isochrones with our data to determine if the 300Myr isochrone was the best choice model for our data. Older isochrone models for ages of 1Gyr and 10Gyr provided turnoff points that occurred too low on the main sequence for our data, while younger isochrones with ages of 10Myr, 30Myr, and 100Myr years had turnoff points that were too high on the main sequence for our data (Figure 11). It should be noted that we kept the same shift in our data when comparing isochrone models as the shift value should not be related to the age of the model, but rather the distance to the cluster. Shifting other models by different amounts, so that their turn-off points approximately matched our cluster, did not produce very good fits with regards to the curve of the main sequence.

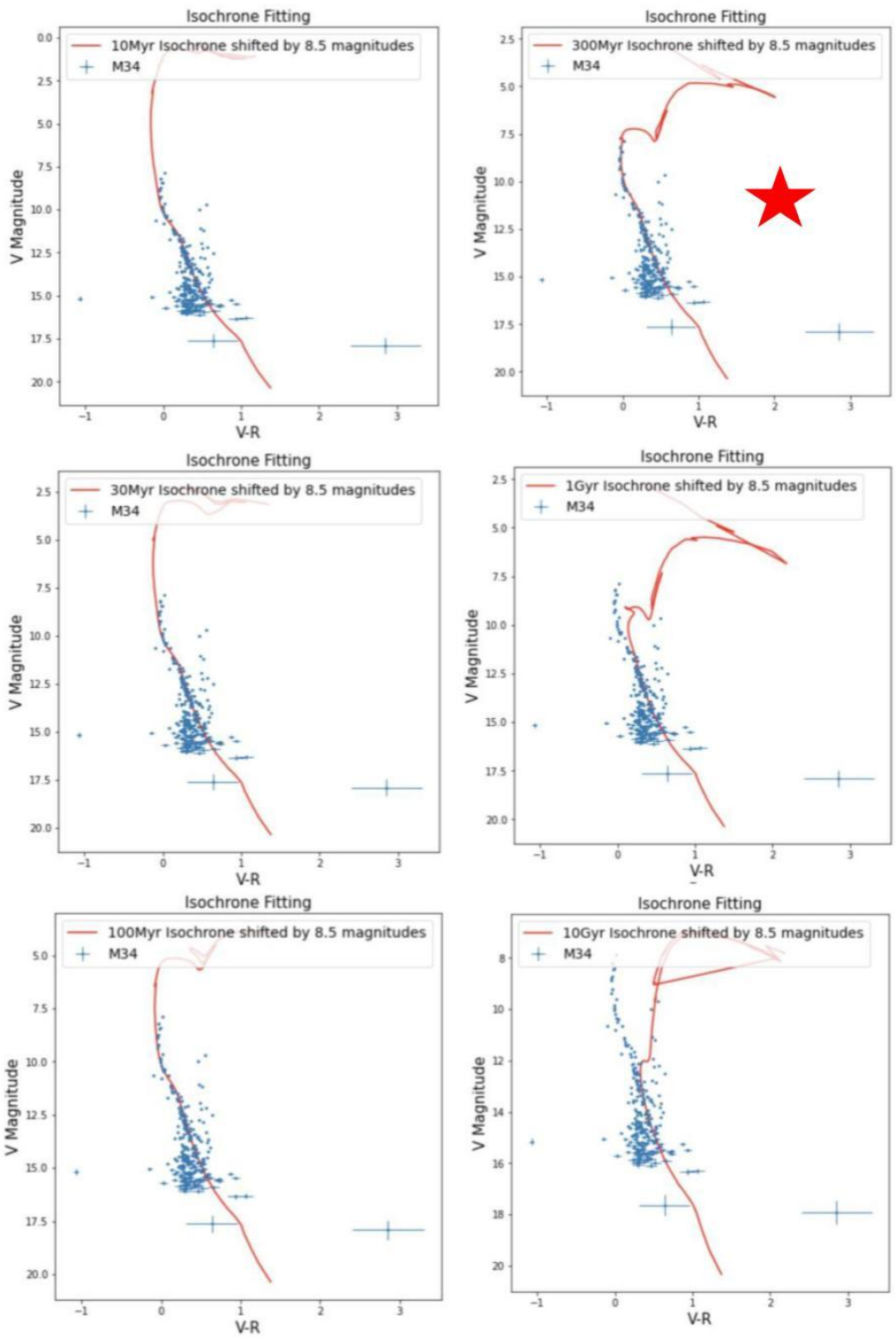

Figure 11

Isochrones of different age are fit to the V-R vs. V CMD of M34. On the left side, the isochrones fitt are 10Myr, 30Myr, and 100Myr years old. On the right side, the isochrones fitted are 300Myr, 1Gyr, and 10Gyr years old. For our particular CMD, the 300Myr isochrone is fit the best. (Indicated by the red star.) The younger isochrones has a main sequence turn off point at lower magnitude. The slope of the CMD at the brightest end is also visibility different from the younger isochrones. The older isochrones have a much shorter main sequence section, and bright stars disappear at much lower luminosity.

Distance determination

Our best fit isochrone needed to be shifted by 8.5 magnitudes in V in order to align with our CMD. Using this value, we can use the distance modulus equation to calculate the distance to our cluster.

$$m - M = 5log(d) - 5$$

This is the distance modulus equation. The value of $m - M$ is equal to the value of the shift in our isochrone, allowing us to solve for d.

$$8.5 = 5log(d) - 5$$
$$13.5 = 5log(d)$$
$$2.7 = log(d)$$
$$10^{2.7} = d$$
$$501.2\ parsec = d$$

For this, we found that the distance to our cluster is equal to 501.2 parsecs. The value for the actual distance to M34 varies, with many online sources citing it as 1500 light years, or 470 parsecs[3]. However, references found through the SIMBAD database provide a distance to M34 of around 499-510 parsecs[4,5]. Comparing our calculated distance value to an actual value of 470 parsecs provides a percent error of 6.6%, while comparing it to the SIMBAD values provides a percent error of 0.42% or 1.72%, depending on if we use the smaller or larger cluster distance value. None of these percent error values are very high, although it does appear our calculated distance value better corresponds to the values provided by SIMBAD. Therefore we can conclude that our distance of 501.2 parsecs is a fairly accurate calculation.

B-V extinction

In an ideal scenario, isochrones would only need to be shifted in the y-axis to fit the CMDs. The shifts in y-axis account for the magnitude difference between absolute magnitude in isochrones and apparent magnitude in CMD. For x-axis, the color of the star we observed should only be determined by the star itself. It should not be affected by the age and the distances of the cluster. However, to perfectly fit the isochrones, shifts in x-axis are needed, meaning that the color of the star in M34 changed. (Figure 12) We think that this change is due to extinction. The effect of Rayleigh scattering (main source of stellar extinction) is more prominent at lower wavelengths, causing the "reddening" of the stars. In our CMDs of M34, the extinction feature is much more prominent in B-V than V-I, as the B filter has the smallest wavelength. By visual inspection, we decided that the B-V extinction is between 0.07 and 0.09. Note that after being corrected for extinction, the isochrone's shift in y-axis also changes to fit the CMD better. In the V vs. B-V CMD, the 300Myr isochrone is shifted by 8 magnitudes to best fit the CMD.

[3] Jones+. (1996). "Membership of Stars in NGC 1039 (M34)".
[4] Kharchenko+. (2005). "Astrophysical parameters of Galactic open clusters".
[5] Dib+ (2018). "Structure and mass segregation in Galactic stellar clusters".

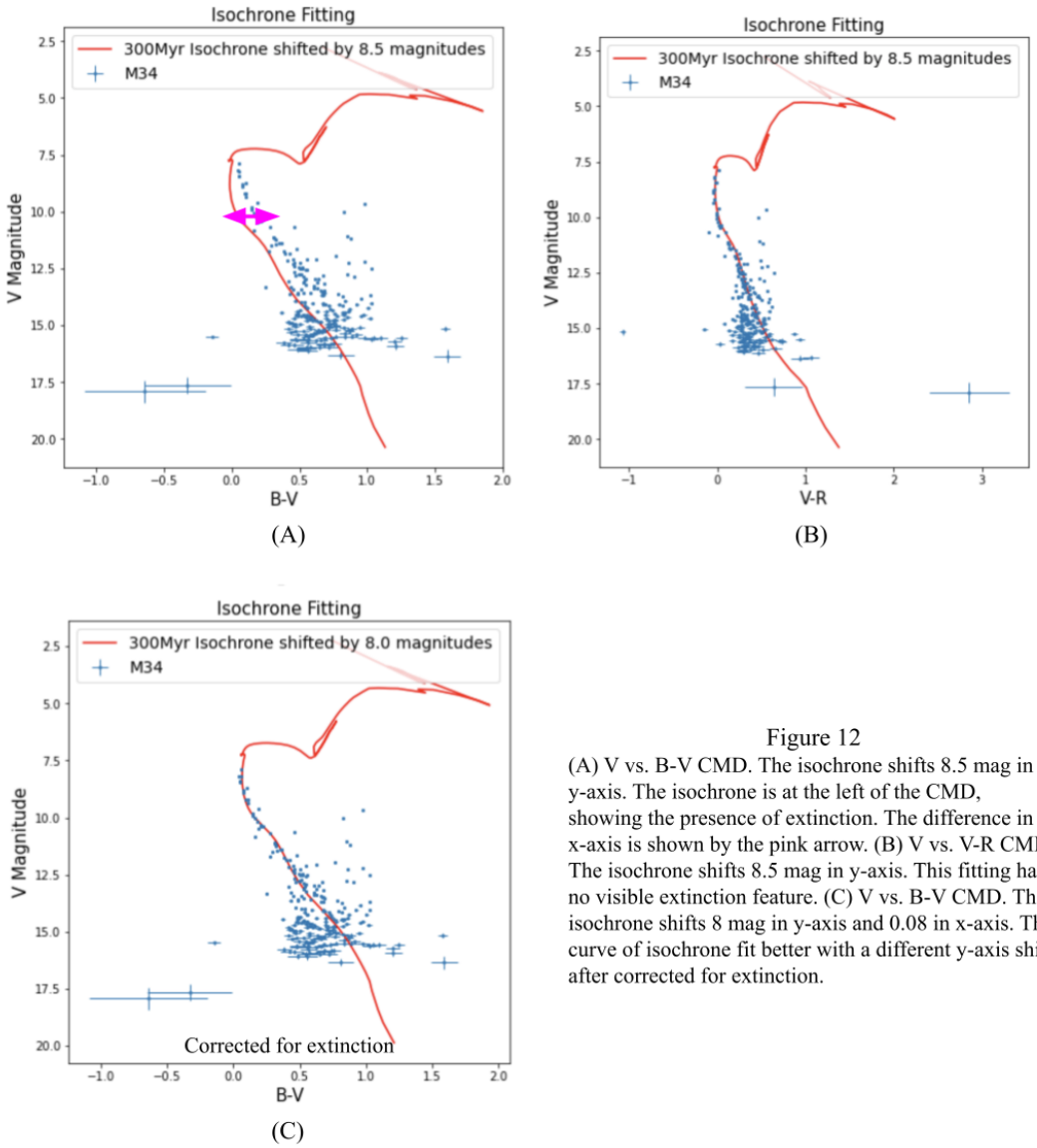

Figure 12
(A) V vs. B-V CMD. The isochrone shifts 8.5 mag in y-axis. The isochrone is at the left of the CMD, showing the presence of extinction. The difference in x-axis is shown by the pink arrow. (B) V vs. V-R CMD. The isochrone shifts 8.5 mag in y-axis. This fitting has no visible extinction feature. (C) V vs. B-V CMD. The isochrone shifts 8 mag in y-axis and 0.08 in x-axis. The curve of isochrone fit better with a different y-axis shift after corrected for extinction.

Possible sources of error

The night of observation was quite windy, and the seeing of the night was roughly 4 arcsec. This is not the best seeing we can have with the Smith 16" telescope. The SNR of all of our data could be lower if the condition were better, and the overall uncertainty on the CMDs would also be lower. In addition, the standard star images in B-band are stretched and blurred due to long exposure time and lack of guide star. We had to manually set a size of the aperture to conduct photometry on the B-band standard star. This causes larger uncertainty on the B-band magnitude of the standard star, and therefore all stars' B-magnitude has a higher error.

The selection of cluster stars would also introduce errors in our final results. We determined a patch of signal to be a star as long as it stood out from its surrounding background. This method may introduce several sources of error in our list of cluster stars. First, bad pixels and random fluctuations around the

edge may be picked up by our algorithm even if they are not stars. These random signals tend to have low pixel values, as it is less likely for many bad pixels to be concentrated in one place. These may account for the low luminosity, large error signals at the bottom of the CMD. We may be able to eliminate these false detections by cutting the edge of the stacked image and adjusting the sigma threshold. However, we would also lose some information. (Figure 13) Faint stars are also likely to have large errors, because their signal-to-noise ratio is low. We were selective in our choice of nsigma while carrying out aperture photometry, which may have meant that some faint stars from M34 were not included in our CMDs.

Other stars may be true detections, but they are not a part of the M34 clusters. These stars may account for the outliers in our CMD. To eliminate these stars, we can cross match our data with the Gaia database[6], and select only the stars that have the same distance to us to be included in the CMD. (Figure 13)

Extinction of the star light as it is scattered by dust in the interstellar medium could introduce uncertainty in isochrone fitting. As discussed earlier in the Results section, after being corrected for extinction, the isochrones may need different shifts in y-axis to better fit the curve of CMD. However, extinction for each color index is different, and it is very hard to determine for longer wavelength filters.

We may find a more accurate result by utilizing more isochrones to fit our data. The current set of isochrones we used have a fairly large difference in age. If more isochrones with smaller age differences are used, we may be able to calculate the age and distance more accurately.

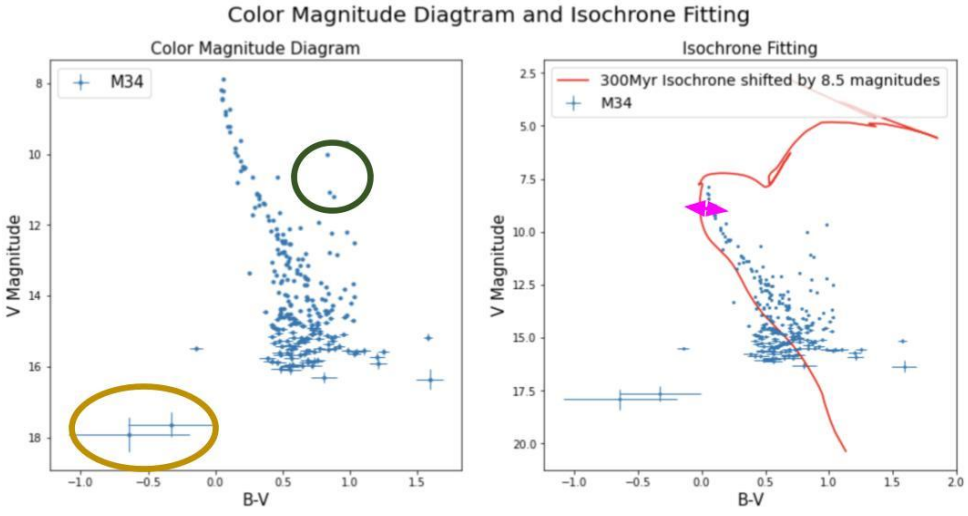

Figure 13

1)The brown circle on the bottom left of the color magnitude diagram shows potential false detections. These "stars" have huge uncertainty with extremely low luminosity. It is very likely that these are bad pixels or random noise we include in our algorithm instead of actual stars. 2) The dark green circle at the top right of the color magnitude diagram shows potential outliers. These stars are true detection, but they may not be the stars from the cluster of interest as they are way off from the cluster's "main sequence." 3) The pink bar in the isochrone fitting graph shows the shift in x-axis (color index) during isochrone fitting. The isochrone have a smaller color index compare to the actual data, indicating that the luminosity in B band is suppose to be higher. This corresponds to higher extinction in higher frequencies.

[6] Gaia DR2 (Gaia Collaboration, 2018)

Conclusions

Using our isochrone fitting we calculated the approximate age for M34 to be 300 Myrs which, compared to the age of our universe, is relatively young. We calculated the approximate distance to the cluster as 501.2pc using isochrone shifting. This is comparable to previously published results. Moreover, M34 is an open cluster that contains both bright and faint stars. When the data was being obtained, we noticed that there were a handful of stars that were very bright, with the brightest star having a visual magnitude of 7.9. Since we wanted to include the faint stars in the cluster as well it is possible that, with the long exposure time, these blue bright stars may have saturated certain pixels and were therefore outliers in our data, specifically on the B band. In addition, when collecting the photometry for our images, we may have registered some data points as stars when they were actually just background values, thus creating outlier data at dimmer magnitudes in our data sets. Future enhancements to this research could be observations on a clearer night with less light pollution or having more finely tuned photometry for our data. Possible future work on our cluster might include studying the metallicity of the cluster to better understand the elements present in the cluster stars.

Citations

Bertelli, G., Bressan, A., Chiosi, C., Fagotto, F., & Nasi, E. (1994, August). Theoretical isochrones from models with new radiative opacities. Astronomy and Astrophysics Suppl., 106, 275-302.

Bessell, M. S. (1990, October). UBVRI passbands. Publications of the Astronomical Society of the Pacific, 102, 1181-1199. doi:10.1086/132749

Dib, S., Schmeja, S., & Parker, R. J. (2018, January). Structure and mass segregation in Galactic stellar clusters. Monthly Notices of the Royal Astronomical Society, 473(1), 849-859. doi:10.1093/mnras/stx2413

European Southern Observatory. (2010, September 9). Landolt Equatorial Standards. https://www.eso.org/sci/observing/tools/standards/Landolt.html

Gaia Collaboration. (2018, August). Gaia Data Release 2. Summary of the contents and survey properties. Astronomy & Astrophysics, 616. doi:10.1051/0004-6361/201833051

Girardi, L. (2021, November 23). CMD 3.6 input form: A web interface dealing with stellar isochrones and their derivatives. http://stev.oapd.inaf.it/cmd

Jones, B. F., & Prosser, C. F. (1996, March). Membership of Stars in NGC 1039 (M34). Astronomical Journal, 111, 1193. doi:10.1086/117865

Kharchenko, N. V., Piskunov, A. E., Röser, S., Schilbach, E., & Scholz, R. (2005, August). Astrophysical parameters of Galactic open clusters. Astronomy and Astrophysics, 438(3), 1163-1173. doi:10.1051/0004-6361:20042523

Landolt, A. U. (1992, July). UBVRI Photometric Standard Stars in the Magnitude Range 11.5 < V < 16.0 Around the Celestial Equator. *Astronomical Journal*, *104*, 340. doi:10.1086/116242

Loidl, R., Lançon, A., & Jørgensen, U. G. (2001, June). Spectra of carbon-rich asymptotic giant branch stars between 0.5 and 2.5 mu m: Theory meets observation. Astronomy and Astrophysics, 371, 1065-1077. doi:10.1051/0004-6361:20010400

Maíz Apellániz, J. (2006, February). A Recalibration of Optical Photometry: Tycho-2, Strömgren, and Johnson Systems. The Astronomical Journal, 131(2), 1184-1199. doi:10.1086/499158

Marigo, P., Girardi, L., Bressan, A., Groenewegen, M., Silva, L., & Granato, G. (2008, May). Evolution of asymptotic giant branch stars. II. Optical to far-infrared isochrones with improved TP-AGB models. Astronomy and Astrophysics, 482(3), 883-905. doi:10.1051/0004-6361:20078467